Numerical modeling of superlattice x-ray-scattering intensities

F. J. Lamelas,* H. David He, and Roy Clarke
Department of Physics, The University of Michigan, Ann Arbor, Michigan, 48109
(Received 6 September 1990; revised manuscript received 16 November 1990)

We describe a one-dimensional x-ray-scattering model that includes discrete layer-thickness fluctuations and interfacial diffusion in the kinematical approximation. We demonstrate the use of the model in an analysis of the out-of-plane scattering intensities of epitaxial Co-Au and Co-Cu superlattices. In the case of Co-Au superlattices, the experimental data show that interfacial diffusion is limited to a two-monolayer region, and that layer-thickness fluctuations are of order ± 1 monolayer. The superlattice features in Co-Cu superlattice measurements are shown to arise from lattice-spacing modulations and are insensitive to composition modulation. The measured intensities are consistent with Co-Cu interfaces which are <2 monolayers thick. A dilation of the Co lattice in the direction of growth is observed for both Co-Au and Co-Cu superlattices. We speculate that the expansion is due to a slightly reduced density of atoms in an imperfectly stacked structure.

INTRODUCTION

X-ray scattering performed in reflection geometry, with the scattering vector normal to the layers, is perhaps the most commonly applied method in the structural analysis of artificially prepared superlattices.[1,2] The basic features of the out-of-plane intensities can be interpreted by inspection, but a more complete analysis of superlattice peak intensities, positions, and widths requires the comparison of measured intensities with those of a realistic scattering model. This is especially true in the case of metallic superlattices, which are far from perfect and require that the scattering model include a variety of types of structural disorder. In this paper we will show how a simple one-dimensional model that incorporates interfacial diffusion and discrete layer-thickness fluctuations is used in fitting the measured out-of-plane scattering intensities from a series of Co-Au and Co-Cu superlattices. Our calculations confirm the abrupt nature of the interfaces in these structures and, in addition, provide evidence for lattice expansions of $\sim 1\%$ along the growth axis.

The diffracted intensities in an out-of-plane scan will consist of peaks at bulk reciprocal lattice points $(2\pi m/d)$ Å^{-1} neighbored by superlattice peaks at spacings of $(2\pi n/\lambda_{SL})$ Å^{-1}, where m,n are integers and d,λ_{SL} are the average periods of the atomic planes and the superlattice bilayers. For a superlattice that is oriented along (hkl) these satellites will occur near the origin, near hkl, near $2(hkl)$, and so on. The features that can be studied through an analysis of out-of-plane scattering intensities include the bilayer thickness, the regularity of the individual layer thicknesses, the sharpness of the interfaces, the lattice parameter along the growth direction, and, to some extent, the epitaxial orientation of the film. Since many of the physical properties of artificial superlattices may be sensitive to the structure of the interfaces, their characterization is of particular importance in these studies. Peak widths in out-of-plane scans (along a radial direction in reciprocal space with the diffraction vector normal to the layers) probe structural coherence along the growth direction, while rocking curve widths are sensitive to both mosaic and the lateral size of domains which scatter coherently. We shall use the low-angle widths as a probe of the coherence of the superlattice layers as a whole; those at high angle are a probe of coherence on an atomic length scale, within the superlattice layers.

In a one-dimensional kinematical approximation one may calculate the out-of-plane scattering amplitude from a layered structure as

$$A(q)=\sum_{n=1}^{M} f_n e^{iqr_n} , \tag{1}$$

where the sum is over each of the M monolayers in the superlattice, f_n is the layer scattering factor (the atomic scattering factor multiplied by the atom density), q is the scattering vector amplitude, and r_n is the position of the nth monolayer. Segmuller and Blakeslee[3] have obtained a closed-form expression for a *step model* of a superlattice which contains n_b bilayers of materials A and B, with N_A and N_B monolayers of A and B in each superlattice bilayer, lattice spacings d_A and d_B, and layer scattering factors f_A and f_B. Their result gives the scattering intensity from an essentially perfect superlattice.

The simplest deviation from an ideal (step-model) superlattice that one might consider is the occurrence of diffusion at the interfaces between the A and B layers. A damping of the higher-order satellite intensities is to be expected since these correspond to the higher-order Fourier coefficients that are necessary in reproducing compositionally abrupt profiles. In the limiting case of a sinusoidal composition profile, only the first-order superlattice satellites will be non-vanishing. On the other hand, since interfacial diffusion does not diminish the long-range order of the superlattice, it does not lead to peak broadening. McWhan *et al.*[4] have developed a

closed-form expression for satellite intensities for the case of trapezoidal composition profiles.

A second type of imperfection to be considered is the occurrence of irregularities in the superlattice layer thicknesses. In the case of a crystallographically ordered superlattice, one may consider *discrete* fluctuations in layer thickness. These are integer-valued variations in the numbers (N_A and N_B) of atomic planes within the superlattice layers. Variations in N_A and N_B that occur across the entire sample may arise from drifts in the deposition rate during superlattice growth. In contrast, local variations in layer thicknesses can originate in the deposition of nonintegral numbers of monolayers. In the case of ordered layer-by-layer growth, the last fractional monolayer deposited on a given layer will consist of an assembly of monolayer-high islands. This effect leads one to expect discrete, local thickness fluctuations of ± 1 monolayer in magnitude. The average size of regions of constant thickness within a layer will be determined by the dynamics of island formation at the metal-vacuum interface. In contrast to discrete layer thickness fluctuations, *continuous* fluctuations will occur when the superlattice includes amorphous layers which can be deposited over a continuous range of thicknesses, or in the case of randomly oriented polycrystalline layers separated by incoherent interfaces. Discrete and continuous fluctuations both give rise to *cumulative* disorder. That is, a variation in the thickness of a given layer in the superlattice will shift the position of all of the layers that are grown subsequently. Such variations will destroy the long-range order of the superlattice, resulting in a finite structural coherence length and diffraction peak broadening.

Sevenhans *et al.*[5] have derived a closed-form expression for the scattering intensity from an amorphous-crystalline superlattice with a continuous Gaussian distribution of amorphous layer thicknesses. When the amorphous layers, which separate successive crystalline layers, have thicknesses that fluctuate on a scale of the atomic plane spacing, phase coherence is lost across crystalline layers. The high-angle diffraction peaks are substantially broadened as the coherence length drops to the thickness of the individual crystalline layers. This model was used to fit the scattering intensities of a polycrystalline-Pb–amorphous-Ge superlattice.[5] Clemens and Gay[6] have extended the analysis of cumulative disorder to the case of discrete fluctuations in layer thicknesses, using a generalized Patterson function method. As in the previous example,[5] they consider layers of an optically dense material separated by layers with zero scattering factor. They find that, in contrast to continuous thickness fluctuations, discrete fluctuations of the order of ± 1 monolayer cause little broadening of the high-angle superlattice satellites. This occurs because the phase shifts associated with discrete fluctuations are not random. In fact, no broadening of the bulk peak will occur when the spacer layers have the same lattice parameter as the dense layers. Clemens and Gay conclude that a condition for the appearance of high-angle superlattice satellites is that the interfaces between the two superlattice constituents must be coherent, in order for the thicknesses of the layers to be confined to integral numbers of atomic plane spacings. Locquet *et al.*[7] combine features of these earlier models and derive an expression for the scattering intensity that simultaneously includes both continuous and discrete fluctuations in layer thicknesses. They have applied their model to the crystalline-crystalline case (in which both constituents of the superlattice are crystalline).

Apart from the question of the effect of discrete versus continuous layer-thickness fluctuations on the high-angle intensities, one can understand the broadening of diffraction peaks at high versus low angles by defining the coherence length as a function of the magnitude of the scattering vector. Consider the integral form of the scattering amplitude:

$$A(q)=\int f(r)\exp(iqr)dr \ .$$

When q corresponds to an allowed reflection, the composition $f(r)$ has a nonvanishing Fourier component at q. For a perfect lattice the contributions to the amplitude integral are in phase across the entire sample, and the coherence length is given by the sample size. On the other hand, when two adjacent blocks within the lattice are displaced by π/q, contributions to the integral from the two blocks will be out of phase. In this case the coherence length is limited to the block size. A criterion for determining the size of regions which scatter coherently is that displacements from the ideally ordered case be less than π/q. Thus we expect that the low-angle (small-q) peaks, which serve as a probe of the superlattice layers as a whole, will be broadened less than the high-angle (large-q) peaks, which probe the local ordering within the superlattice layers.

LAYER SCATTERING MODEL

In our model the calculation of the out-of-plane scattering intensity is carried out by solving Eq. (1) numerically. The problem is reduced to generating the set of scattering factors f_n and layer positions r_n to include in the sum. The thickness of each layer in the superlattice in this case is discrete, given by $N_A d_A$ or $N_B d_B$. One can include layer-thickness fluctuations by allowing N_A and N_B to vary within a fixed distribution. It is also straightforward to include interlayer diffusion by allowing the scattering factors f_n and monolayer spacings $r_n - r_{n-1}$ to vary smoothly at the interfaces. Although this numerical method requires greater computing time than the evaluation of a closed-form expression, it is more flexible since one may generate an arbitrary one-dimensional structure. For example, in contrast to the solutions discussed above,[3–7] we can incorporate layer-thickness fluctuations and interfacial diffusion simultaneously. Since each of these has a different effect on the scattering intensity, it is preferable to include *both* in the analysis of scattering data.

The layered structure that we consider begins as an ideal superlattice of a given chemical composition (set of layer scattering factors f_A, f_B) and lattice parameters d_A, d_B [Fig. 1(a)]. At this point the structure and scattering intensities are equivalent to those of the step model.[3] We note that the scattering factors vary with the scatter-

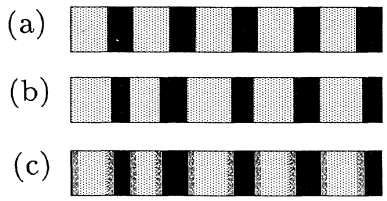

FIG. 1. Illustration of the model used in scattering calculations. (a) Perfect superlattice, (b) disorder in layer thicknesses, and (c) simultaneous disorder in layer thicknesses and interfacial diffusion.

ing angle; in our calculation we express them as a linear function of $\sin\theta/\lambda$. Next we introduce disorder in the layer thicknesses by varying the number of atomic planes in each layer about their average values N_A and N_B [Fig. 1(b)]. The fluctuations in N_A^i and N_B^i (the number of planes of each material in the ith bilayer) are introduced by using a random-number generator to choose N_A^i and N_B^i from a discrete, parabolic layer-thickness distribution. Although we have not done so, one could also add continuous layer-thickness fluctuations by allowing the monolayer spacings $r_n - r_{n-1}$ to fluctuate.

Once layer-thickness fluctuations have been introduced, we include diffusion effects [Fig. 1(c)] by allowing the scattering factors and layer spacings to vary exponentially according to the distance from the nearest interface. For example, the scattering factor of an individual monolayer within the A layer is assigned the value

$$f_n = f_A + \tfrac{1}{2}(f_B - f_A)\exp(-2r'/t_d) ,$$

where r' is the distance from the nearest interface and t_d is the interfacial diffusion width, defined as the distance over which $1-1/e=63\%$ of the composition variation takes place. In the diffusionless limit the scattering factors jump from f_A to f_B in crossing the interface. The atomic plane spacing *at* the AB interface is assumed to be the average plane spacing $\frac{1}{2}(d_A+d_B)$, regardless of the diffusion decay length; away from the interface the spacings follow the same exponential form as the scattering factors. Once the values of d_n and f_n are determined for each atomic plane, at a given scattering angle, the scattering amplitude is calculated using Eq. (1) and squared to give the scattering intensity. Lastly, the scattering intensity is multiplied by Lorentz and polarization factors,[8] and we introduce instrumental broadening by convoluting the calculated intensity with a Gaussian instrumental function.

The introduction of layer-thickness fluctuations destroys the superlattice periodicity; thus the composition profile can no longer be represented by the initial set of Fourier coefficients. Higher-order superlattice peaks are split and/or shifted, as shown in Fig. 2(b). During a particular execution of the program, the fine structure in the scattering intensity is sensitive to the sequence of numbers of atomic planes, N_A^i and N_B^i, that is used in the calculation of the scattering amplitude. The values of N_A^i and N_B^i, in turn, are determined by the sequence of values returned by the random-number generator. On the other hand, a real sample is composed of many local domains within the area sampled by the x-ray beam, each of which contains a different sequence of layer thicknesses. Thus (measured) higher-order superlattice peaks are in general broadened rather than split into a set of sharp peaks. We can simulate this effect in our calculation by averaging intensities over structures which are generated by different sequences of random numbers [Fig. 2(c)].

The total number of bilayers in the superlattice, n_b, is an additional parameter in the calculation of scattering intensities. This parameter has two effects. First, the widths of the diffraction peaks will be broadened to $2\pi/t$, where t is the total thickness of the sample. Secondly, the intensities of the secondary maxima, and the diffuse background in the case of disordered superlattices, are inversely related to the size of the sample, since a perfect sample containing only a few bilayers will contain secondary maxima of significant intensity, while the relative intensities of the secondary maxima vanish as the sample size becomes very large.

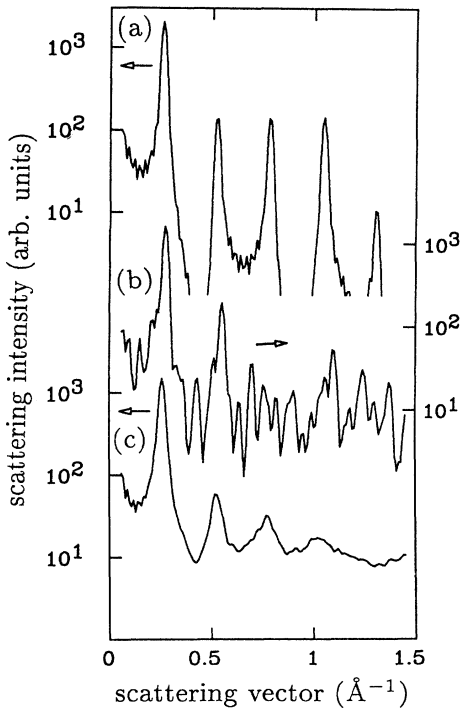

FIG. 2. Effect of layer-thickness disorder on low-angle superlattice scattering intensities. (a) Perfect superlattice with parameters $N_A=5$, $N_B=7$, $d_A=d_B=2.0$ Å, $f_A=0$, $f_B=1$. Low-intensity portions of the curve have been intentionally removed from the plot. (b) Same parameters as (a), but with layer-thickness fluctuations of ±1 monolayer. (c) Same as (b), but with intensities averaged over 100 calculations. All calculations were performed with $n_b=10$ (total) bilayers.

EXPERIMENTAL TECHNIQUES AND RESULTS

The molecular-beam epitaxy (MBE) growth and a variety of structural analyses of these samples have been described previously.[9,10] Their magnetic properties[11] and the details of the growth process[12] are presented elsewhere. Briefly, the superlattices were grown on annealed GaAs (110) substrates at a substrate temperature of 50 °C. Au layers were deposited at a rate of 0.08 Å/sec from a Knudsen cell held at 1300 °C, Cu at 0.5 Å/sec from a cell at 1260 °C, and Co at ~0.3 Å/sec from an electron-beam hearth. The three Co-Au samples which we will discuss have a Au layer thickness of 16 Å and Co thicknesses of 5, 10, and 30 Å. The Co-Cu samples all have a Cu layer thickness of 20 Å, and Co layer thicknesses of 5, 15, and 40 Å. The total superlattice thickness in all cases is ~1500 Å. Out-of-plane x-ray scattering measurements were performed on a four-circle diffractometer, using a 12-kW rotating-Mo-anode x-ray source and a graphite monochromator. The instrumental resolution is primarily determined by the mosaic spread of the graphite monochromator, which is estimated to be ~0.2°.

The measured out-of-plane data for three Co-Au and Co-Cu superlattices are shown in Figs. 3, 4, and 5, along with the intensities calculated with our scattering model. We will detail the intensity calculations below; first we will discuss the measured peak positions, intensities, and widths. The intensities are normalized to counts/sec at a rotating-anode power level of 5.5 kW (55-kV filament-anode potential, 100-mA emission current). The actual counting times were as high as 100 sec/point, depending on count rates and the desired level of statistical accuracy. It is clear that the intensities of the high-angle superlattice satellites in the Co-Au series (Fig. 4) are of the same order of magnitude as those of the bulk peaks, while in the case of Co-Cu (Fig. 5) the satellites are approximately two orders of magnitude weaker than the bulk peaks. Moreover, the low-angle peaks (not shown) are very weak in the Co-Cu series. As we will discuss below, these differences do *not* necessarily imply that the superlattice structure in the Co-Cu series is more disordered or diffuse than in the Co-Au series. Table I lists the peak positions, radial widths (normal to the layers), and rocking curve widths (parallel to the layers), for the data plotted in Figs. 3, 4, and 5. Coherence lengths L are calculated from the radial or rocking curve widths *via* the relation $L=2\pi/\Delta q$, where Δq is the peak width. The last column in Table I contains the superlattice periodicities calculated using the average superlattice peak spacings. We find that the measured periodicities are consistent with the targeted Co and Cu layer thicknesses; however, we estimate that the Au layer thicknesses are actually 20% less than their targeted values (~16 Å, rather than 20 Å).

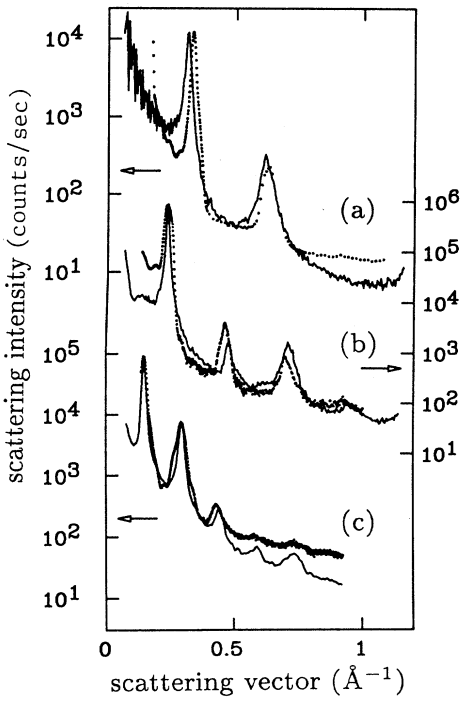

FIG. 3. Measured (points) and calculated (solid curve) low-angle scattering intensities for three Co-Au superlattices. (a) Sample No. 1, with layer thicknesses of 5-Å Co and 16-Å Au; (b) Sample No. 2, with layer thicknesses of 10-Å Co and 16-Å Au; (c) Sample No. 3, with layer thicknesses of 30-Å Co and 16-Å Au.

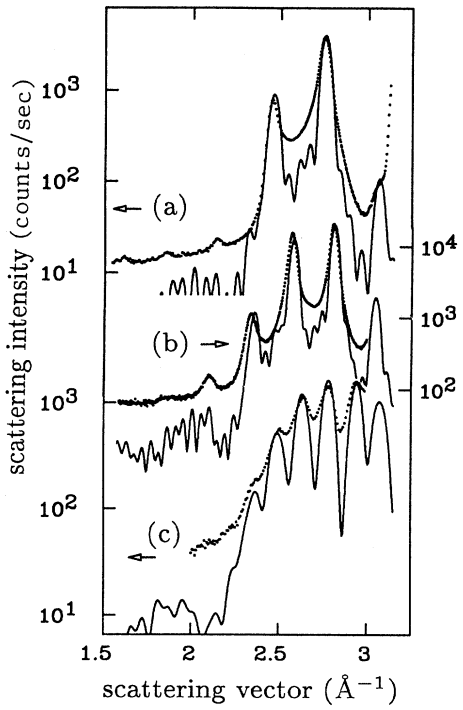

FIG. 4. Measured (points) and calculated (solid curve) high-angle scattering intensities for same three Co-Au superlattices as in Fig. 3.

Given the q dependence discussed above, the lateral coherent domain size derived from rocking curves through high-angle peaks is sensitive to disorder on a length scale of the near-neighbor spacing. In the Co-Au series we obtain a domain size of ~ 35 Å for sample No. 2. This is an estimate of the lateral size of domains within which the atomic planes are ordered vertically to within (π/q_{111}) Å, where $q_{111}=2\pi/d_{111}$. It is interesting to compare this coherence length to the vernier distance, defined as $a^2/(a_A-a_B)$, where a is the average nearest-neighbor spacing and a_A, a_B are the nearest-neighbor spacings of the two elements of the superlattice. For the Co-Au case the nearest-neighbor spacings in the bulk are $a_{Co}=2.50$ Å and $a_{Au}=2.88$ Å; these give a vernier distance of 19.2 Å. On the other hand, the high-angle rocking curve widths may also contain contributions from mosaic effects. Misoriented regions within the superlattice layers could arise in response to the large misfit between the bulk lattices of Co and Au. The Co-Cu high-angle rocking curve widths (sample Nos. 4 and 5) yield lateral domain sizes of ~ 50 Å. These are approximately half of the vernier distance of 108 Å which we obtain from nearest-neighbor spacings of $a_{Co}=2.50$ Å and $a_{Cu}=2.56$ Å. (The instrumental resolution in a rocking curve at high angles corresponds to a lateral coherence length of ~ 1000 Å, and can be neglected here.) The high-angle radial widths, which are measured perpendicular to the layers, are in most cases approximately five times the superlattice period λ_{SL}, with the exception of sample No. 3 where the coherence is only slightly larger than λ_{SL}. For the radial scans at high angle, the instrumental resolution corresponds to a coherence length of ~ 200 Å, a value which is approached in the Co-Cu scans (Table I). Low-angle data are confined to Co-Au samples. Here, the measured lateral domain sizes range from ~ 5000 to $\sim 17\,000$ Å, while the coherence lengths normal to the layers are several hundred Å. Both of these widths, which indicate the structural coherence of the superlattice layers as a whole, approach the instrumental limit. As expected, the q-dependence of the lateral coherence lengths is quite pronounced; the values at the first-order low-angle peak are two orders of magnitude larger than at the bulk peaks.

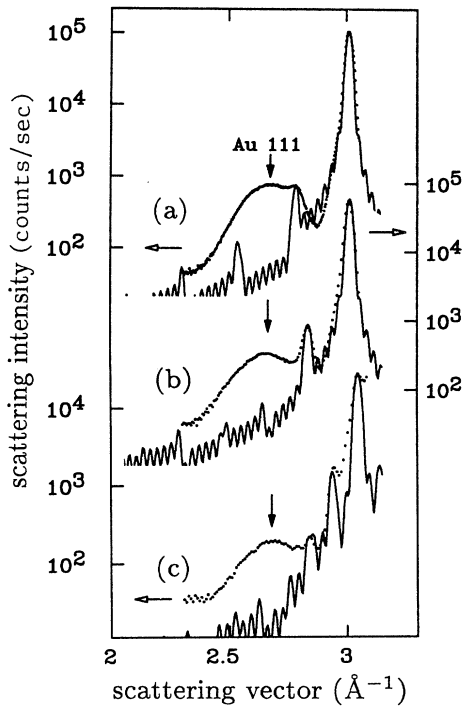

FIG. 5. Measured (points) and calculated (solid curve) high-angle scattering intensities for three Co-Cu superlattices. The broad peak near 2.68 Å^{-1} is due to a 16-Å protective Au layer on the surface of the samples. (a) Sample No. 4, with 5-Å Co layers and 20-Å Cu layers; (b) Sample No. 5, with 15-Å Co layers and 20-Å Cu layers; (c) Sample No. 6, with 40-Å Co layers and 20-Å Cu layers.

In calculating the Co-Au superlattice scattering intensities, we proceed as follows. First of all, we use the nominal layer thicknesses and measured bilayer thicknesses to estimate values of the number of monolayers N_{Co} and N_{Au} to include in each superlattice bilayer. Then we calculate the scattering intensity at low angle for a perfect (nondiffuse and periodic) superlattice while varying N_{Co} and N_{Au}, in order to reproduce the measured *sequence* of peak intensities. Once N_{Co} and N_{Au} have been chosen, the magnitude of the layer-thickness fluctuations ΔN is increased in order to match the widths of the higher-order peaks. Lastly, the interfacial diffusion width t_d is increased; this dampens the higher-order reflections and brings their intensities in line with measured values. The entire process may be repeated a number of times. The total number of bilayers n_b used in the low-angle calculations ranged from the actual number contained in the samples to approximately half that number. In the latter case the reduced value of n_b was used in order to increase the calculated diffuse backgrounds to levels comparable to the measured values. The most important smoothing of the calculated low-angle intensities was carried out by averaging intensities after repeated iterations of the scattering calculation [as illustrated in Fig. 2(c)]. Typically, an average over 100 intensity calculations produced satisfactory results. During the fitting process, the calculated intensities are multiplied by a scaling constant and displayed on a semilog plot along with the measured intensities.

Table II lists the parameters used in calculating the scattering intensities shown in Figs. 3–6. The first three rows of the table correspond to the low-angle Co-Au superlattice intensities. The numbers of monolayers N_{Co} and N_{Au} are in reasonable agreement with the individual layer-thickness estimates made on the basis of the measured superlattice periods. The total number of bilayers included in the calculation, n_b, was in one case [Fig. 3(b)] equal to and in two cases [Figs. 3(a) and 3(c)] approxi-

TABLE I. Measured peak positions, radial widths, radial coherence lengths, rocking curve widths, and lateral coherence lengths obtained from the data shown in Figs. 3–5.

Sample Number	q (Å^{-1})	Δq_{rad} (Å^{-1})	$\frac{2\pi}{\Delta q_{\text{rad}}}$ (Å)	Δq_{rock} (Å^{-1})	$\frac{2\pi}{\Delta q_{\text{rock}}}$ (Å)	λ_{SL} (Å)
1	0.329	0.016	390	0.000 373	16 900	
(5-Å Co)-(16-Å Au)	0.625	0.050	126	0.008 79	715	
	2.453	0.069	91			
	2.749	0.064	98			21.2
2	0.236	0.028	226	0.000 433	14 500	
(10-Å Co)-(16-Å Au)	0.465	0.027	232			
	0.700	0.040	157			
	2.339	0.073	86			
	2.569	0.047	135			
	2.803	0.043	147	0.176	35.7	27.1
3	0.149	0.020	317	0.001 08	5830	
(30-Å Co)-(16-Å Au)	0.296	0.033	189			
	0.433					
	2.640					
	2.781	0.122	52			
	2.941					43.0
4	2.788					
(5-Å Co)-(20-Å Cu)	3.010	0.035	180	0.121	52.0	28.3
5	2.836	0.055	114			
(15-Å Co)-(20-Å Cu)	3.010	0.035	180	0.131	47.9	36.1
6	2.839					
(40-Å Co)-(20-Å Cu)	2.944					
	3.049					59.8

mately half of the actual number of bilayers in the sample. In the latter case the superlattice is treated as a sum of two regions which scatter independently. Since the low-angle intensities are not sensitive to ordering on a length scale of the nearest-neighbor distance, we did not alter the lattice parameters of the Co or Au layers in these calculations, as indicated in the last two columns of the table. The parameters that are most significant in these calculations are t_d, the diffusion layer thickness, and ΔN, the layer-thickness distribution width. We find that the measured intensities are consistent with values of $t_d = \sim 1.4$ monolayers, and with layer-thickness fluctuations ranging from ± 0.6 to ± 1.2 monolayers. It is to be noted that a one-dimensional model cannot be used to distinguish interfaces which are truly diffuse from those which contain an array of steps. In the latter case the interfaces could be atomically abrupt *locally,* while appearing diffuse when the composition is averaged laterally over distances larger than the step spacing. This averaging occurs since the coherent scattering intensity arises

TABLE II. Parameters used in calculating the intensities shown in Figs. 3–6. These are N_{Co} and $N_{\text{Au/Cu}}$, the numbers of Co and Au or Cu monolayers in each bilayer; n_b, the total number of bilayers in the structure; Δq_{in}, the instrumental width; n_{ave}, the number of calculations over which the intensities are averaged; t_d, the diffusion layer width in monolayers; ΔN, the width of the layer-thickness distribution; and Δd_{Co}, $\Delta d_{\text{Au/Cu}}$, the strains (in %, relative to the bulk value) in the monolayer spacings.

Figure	$N_{\text{Co,Au/Cu}}$	n_b	Δq_{in} (Å^{-1})	n_{ave}	t_d	ΔN	Δd_{Co} (%)	$\Delta d_{\text{Au/Cu}}$ (%)
3(a)	3,6	25	0.004	100	1.3	1.2	0	0
3(b)	6,6	50	0.004	100	1.5	1.2	0	0
3(c)	15,5	15	0.012	100	1.3	2.4	0	0
4(a)	3,6	5	0.020	5	1.3	1.2	1.7	1.3
4(b)	6,6	5	0.020	5	1.5	1.2	2.0	1.5
4(c)	14,6	2	0.020	5	1.3	2.4	0.7	0.9
5(a)	3,10	8	0.020	1	0	0	0.7	0.5
5(b)	7,10	6	0.020	1	0	0	1.2	0.7
5(c)	20,10	3	0.020	1	0	0	0.5	0.5
6(a)	7,10	6	0.020	1	0	0	0	0
6(b)	7,10	6	0.020	1	0	0	2.6	0

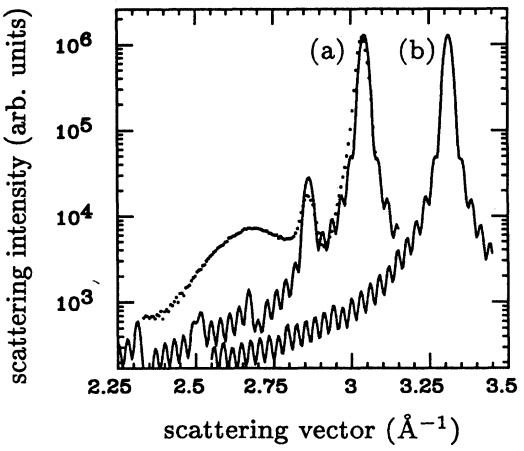

FIG. 6. The effect of relative strains on Co-Cu superlattice peak intensities. The points are the measured values for sample No. 5 [same as Fig. 5(b)], while the solid curves are the calculated intensities for perfect (nondiffuse) superlattices. Curve (a) was obtained with d_{Co} and d_{Cu} set to their bulk values. Curve (b) (displaced for clarity) was obtained using $d_{Co}=d_{Cu}$.

from an assembly of atoms within regions of a size given by the coherence length. At low angles, this length is at least several hundred angstroms (Table I). Complementary methods such as NMR (Ref. 13) may be useful in determining the local environment at the interface. In any case, our results indicate that the interfaces in these Co-Au superlattices are confined to a two-monolayer region.

Next, we turn to the procedure used in fitting the high-angle Co-Au data. First, we note that the measured high-angle widths are significantly larger than at low angle, since, as we have mentioned above, the structural coherence length is q dependent. The most realistic way to account for this effect would be to include continuous layer-thickness fluctuations by allowing the monolayer spacing $r_n - r_{n-1}$ to fluctuate with a small amplitude. However, for simplicity, in our calculation we reproduce the high-angle widths by reducing n_b, the number of bilayers in the superlattice. This method broadens all reflections due to the (artificially small) finite size of the superlattice. The coherent scattering length, equal to the finite size, is $n_b\lambda_{SL}$.

Next, we calculate the high-angle scattering intensity using the same parameters as at low angle (apart from the reduced value of n_b). This generally results in relative peak intensities that are close to the measured values; however, the entire (calculated) spectrum is shifted to q values that are approximately 0.05 Å^{-1} higher than the measured values. This shift is considerably greater than any sytematic experimental error, which is estimated to be at most 0.1° in 2θ (0.015 Å^{-1}). That is, the measured spectra correspond to superlattices with perpendicular interatomic spacings that are somewhat greater than the bulk values of Co and Au. After adjusting the Co and Au monolayer spacings, a satisfactory fit is obtained (Fig. 4).

The superlattice satellite intensities are sensitive to lattice-spacing modulations as well as to composition modulations: When the Co and Au atomic plane spacings are brought closer together, the satellite intensities drop, relative to the bulk peak, and *vice versa*. However, an equal shift of *both* lattice parameters produces a shift in q of the calculated intensities with no appreciable change in the relative peak intensities. The curves shown in Fig. 4 were obtained with *both* the Co and Au layers expanded along the growth axis; however, the expansions are asymmetric in order to provide small adjustments in the relative satellite intensities (see Table II). Previous studies[11] have shown that the Co layers are expanded (by 1–2 %) and the Au layers are compressed (by ~1%) in the plane of the superlattice. The in-plane measurements[11] led us to expect an expansion of the Au layers and a contraction of the Co layers, along the growth direction. Thus, the out-of-plane expansion of the Co layers is unexpected.[14]

As we have noted above, a better model of the high-angle scattering intensities would include continuous layer-thickness fluctuations. Such fluctuations would produce the observed high-angle peak broadening and would also affect the the high-angle satellite intensities. In the present case, the strain values given in Table II were chosen in order to match peak intensities, as well as the peak shifts. Since the intensities would be affected by the presence of continuous fluctuations, the perpendicular strain values indicated by our fitting of the high-angle data may not be very accurate. Nevertheless, it is apparent that a significant ($\gtrsim 1\%$) expansion of the average Au and Co monolayer spacing is necessary in order to produce the correct shift in the calculated spectra to lower values of q, although we cannot assign accurate strain values to the *individual* layers of the superlattice. As noted above, an out-of-plane expansion of the Au layers is not surprising, given their in-plane contraction. An out-of-plane expansion of the Co layers, on the other hand, cannot be understood in terms of an elastic deformation in response to epitaxial strains at the superlattice interfaces. The Co layer expansion could arise as a result of structural defects originating at the interfaces. That is, structural disorder within the Co layers may inhibit the ideal packing of one plane of atoms upon another, leading to an effectively larger spacing between the (close-packed) Co planes. We discount the alloying of Co with Cu or Au as an explanation for the apparent Co lattice expansion since Co is almost completely immiscible with Cu and Au. Furthermore, NMR measurements[13] have indicated that the Co-Cu interface is atomically abrupt.

Scattering intensities from Co-Cu superlattices at high angle are shown in Fig. 5. There is a very poor contrast in scattering factors between Co and Cu, due to their nearly adjacent positions in the Periodic Table. In Fig. 6 we plot the intensities from a step model (with no layer-thickness fluctuations or interfacial diffusion), along with the measured intensities for sample No. 5. When the Co and Cu lattices take on their bulk lattice parameters [Fig. 6(a)], we obtain a superlattice satellite that is somewhat more intense than the measured one. However, when the lattice parameter of Co is set equal to that of Cu [Fig. 6(b)], the satellite vanishes. Thus the Co-Cu superlattice

features arise primarily from lattice-spacing modulations and are insensitive to composition modulation *per se*. It is for this reason that we restrict the Co-Cu fitting procedure to modifications of the lattice spacings d_{Co} and d_{Cu} (Fig. 5). As described above, an equal shift of the Co and Cu spacings shifts the entire pattern, while an asymmetric shift alters the superlattice satellite intensities, relative to the bulk peak intensity. For Co-Cu, the in-plane data[10] show that the Co layer strains are tensile, and those of the Cu layers are compressive, leading one to expect an out-of-plane expansion of Cu and compression of Co. However, as in the Co-Au case, we find that our measurements are consistent with an out-of-plane expansion of both the Co and Cu lattices. The calculated intensities (Fig. 5) were obtained with expansions that are slightly asymmetric and range from 0.5% to 1.2% (Table II).

CONCLUSIONS

We find that a simple model for the scattering intensity from layered structures is quite useful in the analysis of out-of-plane x-ray-scattering data from metallic superlattices. The incorporation of both diffusion and thickness fluctuations into the model is particularly important when analyzing superlattices that deviate significantly from the ideal. This will usually be the case for metallic superlattices with very thin ($\lesssim 10$ Å) layers, where the interface thickness may approach the layer thickness. By applying this model to Co-Au superlattices, we are able to characterize the interfaces as being confined to a two-monolayer region. In addition, we find that the Co layers are apparently expanded along the growth direction, most likely as a consequence of structural disorder which leads to a slight decrease in the packing density. Measurements of Co-Cu superlattices are made more difficult due to their nearly equal atomic numbers; however, here our results are at least consistent with the Co-Au results, in terms of both the interface smoothness and the apparent lattice expansion along the growth direction.

ACKNOWLEDGMENTS

We would like to thank W. Vavra and C. H. Lee for their help during the growth of these samples. Eric Fullerton was helpful in discussing his scattering calculations with us. This work was supported in part by National Science Foundation (NSF) Grant No. DMR 8805156. One of us (F.L.) was supported in part by the U.S. Army Research Office.

*Present address: AT&T Bell Laboratories, Murray Hill, NJ 07974.

[1]D. B. McWhan, in *Physics, Fabrication, and Applications of Multilayered Structures,* edited by P. Dhez and C. Weisbuch, (Plenum, New York, 1988).

[2]Y. Fujii, in *Metallic Superlattices,* edited by T. Shinjo and T. Takada (Elsevier, Amsterdam, 1987).

[3]A. Segmuller and A. E. Blakeslee, J. Appl. Cryst. **6**, 19 (1973).

[4]D. B. McWhan, M. Gurvitch, J. M. Rowell, and L. R. Walker, J. Appl. Phys. **54**, 3886 (1983).

[5]W. Sevenhans, M. Gijs, Y. Bruynseraede, H. Homma, and I. K. Schuller, Phys. Rev. B **34**, 5955 (1986).

[6]B. M. Clemens and J. G. Gay, Phys. Rev. B **35**, 9337 (1987).

[7]J.-P. Locquet, D. Neerinck, L. Stockman, Y. Bruynseraede, and I. K. Schuller, Phys. Rev. B **39**, 13 338 (1989).

[8]A. Guinier, *X-ray Diffraction in Crystals, Imperfect Crystals, and Amorphous Bodies* (Freeman, San Francisco, 1963).

[9]C. H. Lee, Hui He, F. Lamelas, W. Vavra, C. Uher, and Roy Clarke, Phys. Rev. Lett. **62**, 653 (1989).

[10]F. J. Lamelas, C. H. Lee, Hui He, W. Vavra, and Roy Clarke, Phys. Rev. B **40**, 5837 (1989).

[11]C. H. Lee, H. David He, F. J. Lamelas, W. Vavra, C. Uher, and Roy Clarke, Phys. Rev. B **42**, 1066 (1990).

[12]H. David He, Ph.D. thesis, University of Michigan, 1990.

[13]Atomically abrupt interfaces in Co-Cu superlattices have been indicated by the observation of interface features in spin-echo NMR measurements, described elsewhere: K. Le Dang, P. Veillet, H. David He, F. J. Lamelas, C. H. Lee, and Roy Clarke, Phys. Rev. B **41**, 12 902 (1990).

[14]Out-of-plane lattice expansions were reported in earlier studies of sputtered polycrystalline Mo-Ni superlattices [Mahbub R. Khan, C. S. L. Chun, G. P. Felcher, M. Grimsditch, A. Kueny, Charles M. Falco, and Ivan K. Schuller, Phys. Rev. B **27**, 7186 (1983)] and Nb-Cu superlattices [Ivan K. Schuller and M. Grimsditch, J. Vac. Sci. Technol. B **4**, 1444 (1986)]. However, in these cases no in-plane x-ray data were available for comparison and the analysis of the out-of-plane data was not as extensive as in this paper.